

**Supplementary information**

**Effects of Néel and Brownian relaxations on dynamic magnetization empirically characterized in  
single-core and multicore structures of magnetic nanoparticles**

Haruki Goto<sup>a</sup>, Masato Futagawa<sup>b</sup>, Yasushi Takemura<sup>c</sup> and Satoshi Ota<sup>b\*</sup>

<sup>a</sup> *Department of Optoelectronics and Nanostructure Science, Graduate School of Science and Technology, Shizuoka University, Hamamatsu 432-8561, Japan*

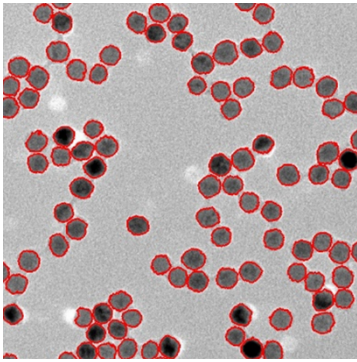
<sup>b</sup> *Department of Electrical and Electronic Engineering, Shizuoka University, Hamamatsu 432-8561, Japan*

<sup>c</sup> *Department of Electrical and Computer Engineering, Yokohama National University, Yokohama 240-8501, Japan*

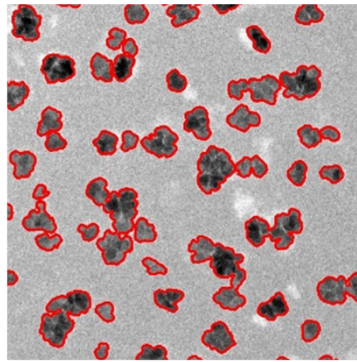
\*E-mail: ota.s@shizuoka.ac.jp

### **Supplementary Note S1: Analysis of diameters in measured magnetic nanoparticles**

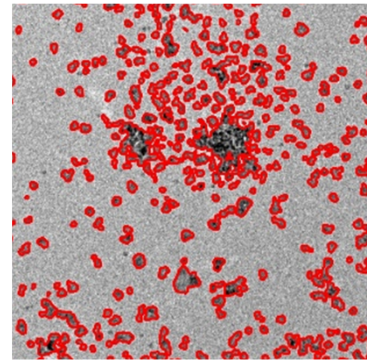
The particle diameter was calculated using the OpenCV Python module, based on TEM images. The analysis involved binarizing the TEM images to detect particle contours. Next, the findContours function in OpenCV was applied for contour detection. The area within each detected contour was then calculated by counting pixels. Finally, the particle diameter was derived from this calculated area, assuming that the particles were spherical. Fig. S1 illustrates the typical output from the findContours function for each particle. In the SHA-20 sample, contours enclosing two or more particles as shown in Fig. S2 were excluded as false positives.



SHA-20

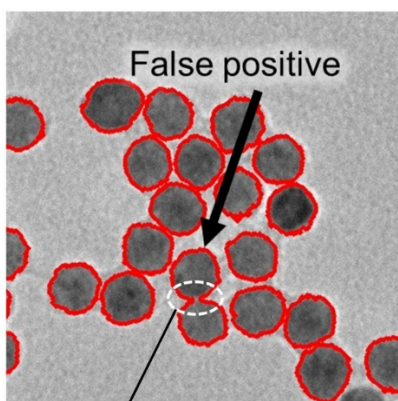


Synomag<sup>®</sup>-D



Resovist<sup>®</sup>

Fig. S1 Example of TEM image analysis



A contour enclosing  
two particles

Fig. S2 Example of false positive in SHA-20.

### Supplementary Note S2: Estimation of the effective core diameter

To estimate the distribution of the effective core diameter, the DC magnetization curves in the liquid sample were fitted using the Langevin function:

$$L_{cal}(H) = \sum_{i=1}^{N_{A,M}} A_{V,M,i} \left\{ \coth(\xi_i) - \frac{1}{\xi_i} \right\}, \#(S1)$$

where  $\xi = \mu_0 M_s V_M H / k_B T$ ,  $A_{M,V}$  denotes the volume fraction of the magnetic moment  $M_s V_M$ ,  $\mu_0$  is the permeability in free space,  $M_s$  is the saturation magnetization of the MNPs,  $V_M$  is the core volume of the MNPs,  $k_B$  is the Boltzmann constant,  $T$  is the temperature, and  $N_{A,M}$  denotes the number of points in  $A_{V,M}$  whose sum is 1. In the estimation approach, the magnetization curves were normalized by the magnetization value at  $H = 1.26$  T. As training data to be fed into a neural network (NN),  $L_{cal}$  values were prepared by calculating  $A_{V,M}$  from the sum of three randomly selected Gaussian distributions with  $-22.0 < \log_{10}(M_s V_M) < -16.0$  using Eq. (S1).

A deep learning framework was designed as shown in Fig. S3.<sup>2</sup> The MSE was calculated as

$$MSE = \sum_{i=1}^{N_{train}} \left\{ \sum_{j=1}^{N_{out}} (A_{V,M,pred,i,j} - A_{V,M,train,i,j})^2 + \alpha_L \sum_{j=1}^{N_{in}} (L_{cal,pred,i,j} - L_{cal,train,i,j})^2 \right\} / N_{train}, \quad (S2)$$

where  $\alpha_L$  is a coefficient that controls the weight of the factors associated with the calculated loss ( $\alpha_L = 0.01$ ). The “pred” and “train” indices indicate parameters representing the data predicted after training and training data, respectively, with  $N_{train}$ ,  $N_{in}$ , and  $N_{out}$  representing the number of training, input, and output data points. The predicted  $L_{cal}$  was calculated with Eq. (S1) using the predicted  $A_{V,M}$ . After the weights in the hidden layer of the NN were adjusted, the experimental  $A_{V,M}$  was analyzed by inputting the measured magnetization curve.  $A_{M,V}$  was applied as the effective core diameter distribution given by  $M_s V_M$  and the measured mean  $M_s$  assuming a spherical particle approximation.

We employed the Adabelief optimizer,<sup>3</sup> and the NN model was trained using the open framework Pytorch with CUDA 11.8 on an NVIDIA Titan V graphic processing unit (GPU).

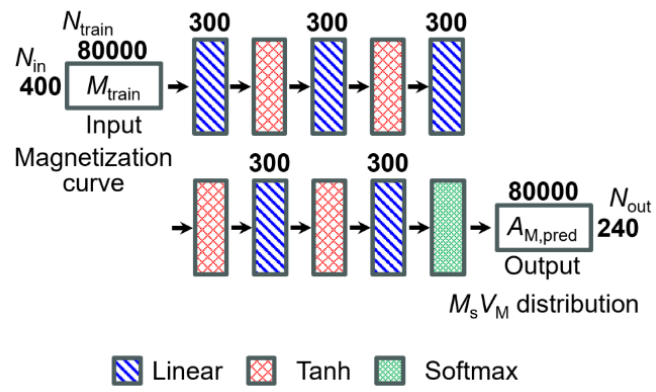


Fig. S3 Deep learning framework for estimating distributions of the magnetic moment  $M_s V_M$  from magnetization curves.

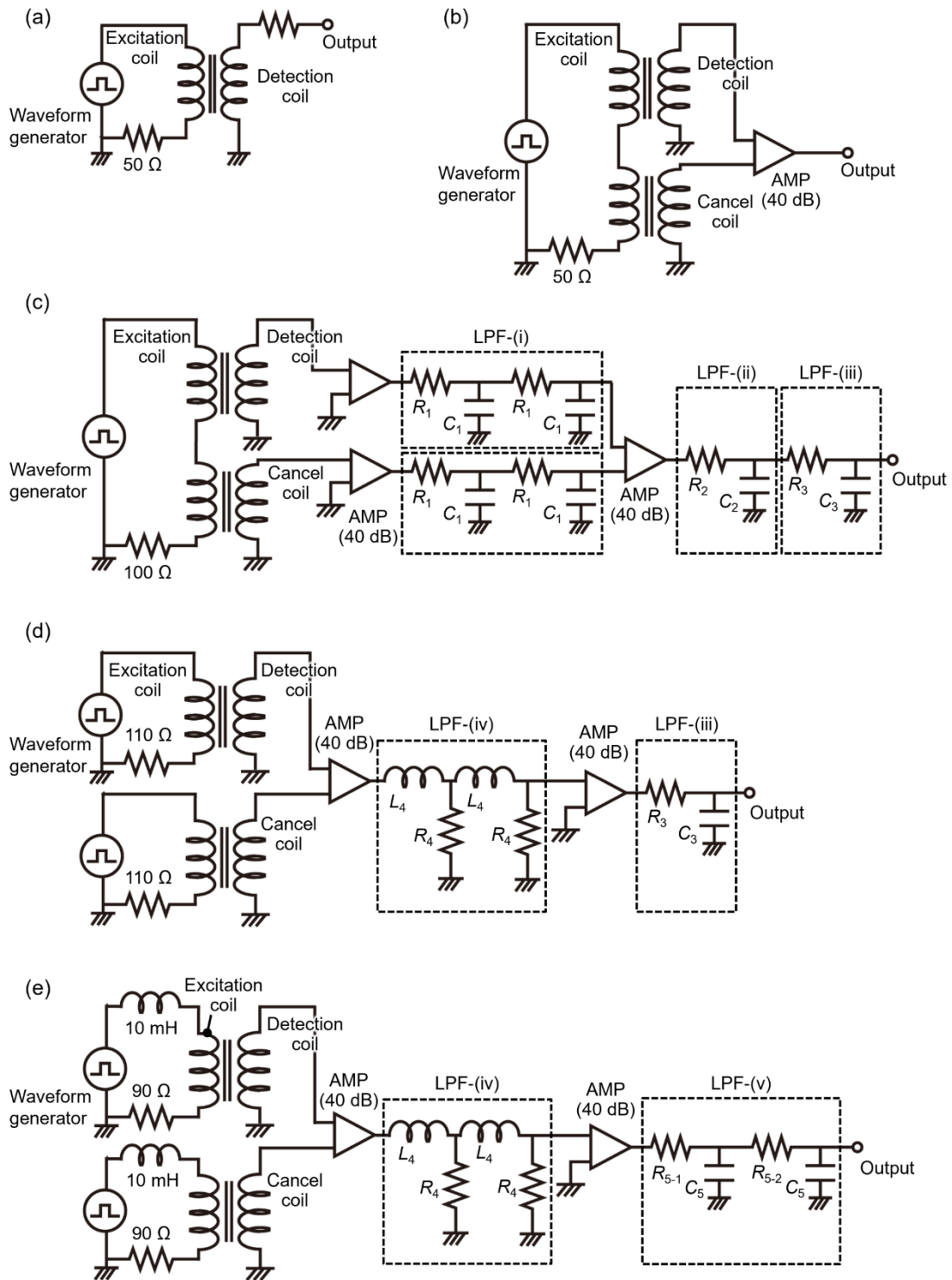


Fig. S4 Measurement circuit of (a) circuit-(i), (b) circuit-(ii), (c) circuit-(iii), (d) circuit-(iv), and (e) circuit-(v) shown in Table S1. Low pass filters (LPFs) consisting of a resistor and capacitor and a set of inductors and resistors were mounted in the circuits.  $R_1 = 50 \Omega$  and  $C_1 = 680 \text{ pF}$  in LPF-(i),

$R_2 = 55 \Omega$  and  $C_2 = 34.5 \text{ nF}$  in LPF-(ii),  $R_3 = 50 \Omega$  and  $C_3 = 4.7 \text{ nF}$  in LPF-(iii),  $L_4 = 10 \text{ mH}$  and  $R_4 = 1.1 \text{ k}\Omega$  in LPF-(iv), and  $R_{5-1} = 100 \Omega$ ,  $R_{5-2} = 50 \Omega$ , and  $C_5 = 1.68 \mu\text{F}$  in LPF-(v) were applied.

Table S1 Number of turns  $N_{\text{coil}}$  and diameter of copper wire  $d_{\text{wire}}$  for excitation and detection coils in each circuit.

Circuit		( i )	( ii )	( iii )	( iv )	( v )	( vi )	( vii )
Excitation coil	$d_{\text{wire}}$ [mm]	0.06	0.06	0.3	0.3	0.3	0.06	0.06
	$N_{\text{coil}}$ [turn]	5 × 10 layer	5 × 10 layer	60	60	100	5 × 10 layer	5 × 10 layer
Detection coil	$d_{\text{wire}}$ [mm]	0.06	0.06	0.06	0.04	0.04	0.06	0.06
	$N_{\text{coil}}$ [turn]	1	4	100	360	2400	2	4

Table S2 Appropriate time when magnetization was normalized with each magnetic relaxation process measured by the different circuits in each period.

Circuit	( i )	( i )	( ii )	( iii )	( iv )	( v )	
Rise time of applied magnetic field	18 ns	80 ns	270 ns	23 $\mu$ s	1 ms	18 ms	
SHA-20	$\eta = 0.89$ mPa·s	2.2 $\mu$ s	–	75 $\mu$ s	~ 10 ms	–	–
	$\eta = 5.4$ mPa·s	2.0 $\mu$ s	–	284 $\mu$ s	~ 10 ms	–	–
	$\eta = 12.4$ mPa·s	385 ns	–	65 $\mu$ s	14 ms	~ 130 ms	–
	Solid	126 ns	1.2 $\mu$ s	38 $\mu$ s	1.2 ms	34 ms	~200 ms
	$\eta = 0.89$ mPa·s	2.2 $\mu$ s	–	67 $\mu$ s	~ 10 ms	–	–
Synomag®-D	$\eta = 5.4$ mPa·s	2.0 $\mu$ s	–	77 $\mu$ s	~ 10 ms	–	–
	$\eta = 12.4$ mPa·s	960 ns	–	68 $\mu$ s	~ 10 ms	–	–
	Solid	103 ns	1.1 $\mu$ s	35 $\mu$ s	2.0 ms	43 ms	~200 ms
	$\eta = 0.89$ mPa·s	1.0 $\mu$ s	–	50 $\mu$ s	~ 10 ms	–	–
Resovist®	$\eta = 5.4$ mPa·s	1.0 $\mu$ s	–	50 $\mu$ s	~ 10 ms	–	–
	$\eta = 12.4$ mPa·s	441 ns	–	60 $\mu$ s	14 ms	~130 ms	–
	Solid	100 ns	1.8 $\mu$ s	61 $\mu$ s	4.5 ms	78 ms	~200 ms

### **Supplementary Note S3: Excitation magnetic fields and magnetic relaxation processes measured by different circuits**

Owing to the slow response of magnetization, the measurement period was limited to 200 ms. The magnetic relaxation processes measured by different circuits were normalized to align magnetization at each applicable time, as shown in Table S2. Fig. S5 presents the excitation magnetic fields and magnetic relaxation process measured across three different circuits at  $\eta = 0.89$  mPa·s.

To convert the magnetic flux measured by the detection coil of circuit-(v) under a pulsed magnetic field,  $\Phi_{\text{pulse}}$ , into the absolute magnetization per unit weight,  $M_{\text{pulse}}$ , specific steps were followed. For MNPs in liquid samples and Synomag<sup>®</sup>-D in solid form, where magnetic relaxation was essentially complete at 200 ms, the maximum  $\Phi_{\text{pulse}}$  was directly converted into magnetization values obtained via VSM at 0.1 mT. Conversely, for SHA-20 and Resovist<sup>®</sup> in solid form, where magnetic relaxation was incomplete at 200 ms,  $\Phi_{\text{pulse}}$  was converted into  $M_{\text{pulse}}$  by applying a ratio of  $(M_{\text{VSM}} \text{ at } 0.1 \text{ mT}) / (\Phi_{\text{pulse}} \text{ at } 200 \text{ ms})$ , preliminarily determined from the single-core MNPs of SHA-15 (Ocean NanoTech Ltd., San Diego, CA, USA) in solid form, as shown in Fig. S6, where the magnetic relaxation was substantially completed at 200 ms.<sup>4</sup> The percentage of  $M_{\text{pulse}}$  at 200 ms for the incomplete magnetic relaxation in SHA-20 and Resovist<sup>®</sup> was estimated by  $(M_{\text{pulse}} \text{ at } 200 \text{ ms}) / (M_{\text{VSM}} \text{ at } 0.1 \text{ mT})$ . The  $M_{\text{VSM}}$  at low magnetic fields for SHA-20 and Resovist<sup>®</sup> are shown in Fig. S7.

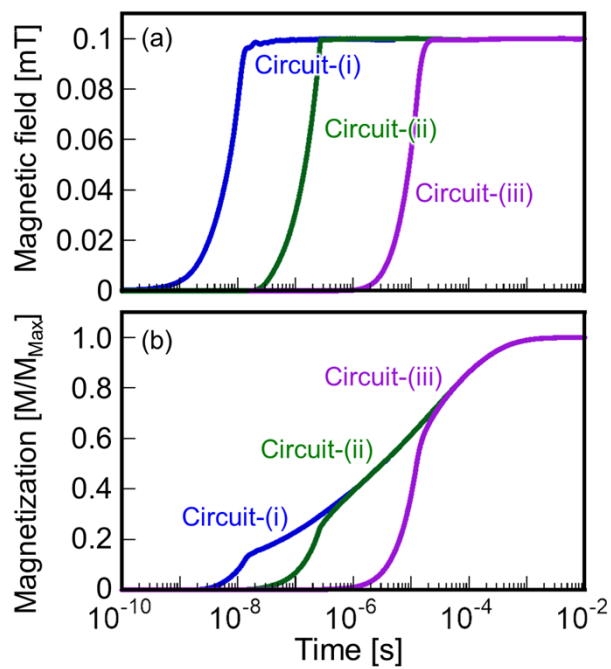


**Fig. S5** (a) Applied pulsed magnetic field and (b) measured magnetic relaxation process of MNPs in three different circuits in each measurement period with respect to Synomag<sup>®</sup>-D in  $\eta = 0.89$  mPa·s as shown in Table S2 as an example.

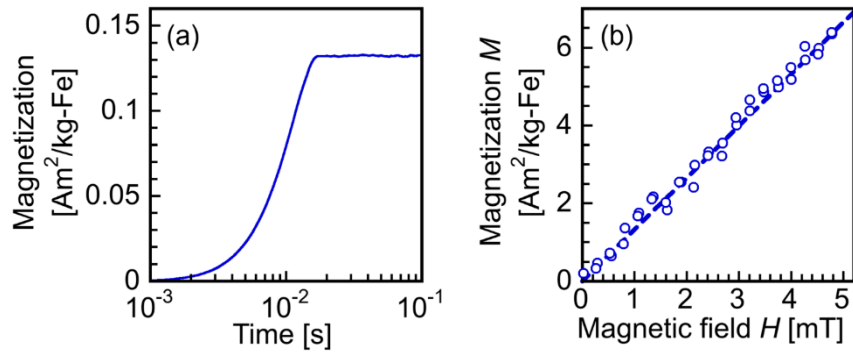


**Fig. S6** (a) Magnetic relaxation response measured by circuit-( v ), and (b) magnetization curve measured under DC magnetic field for 0–5 mT (plots) and linear approximation of these plots (dotted line) in SHA-15 in the solid.

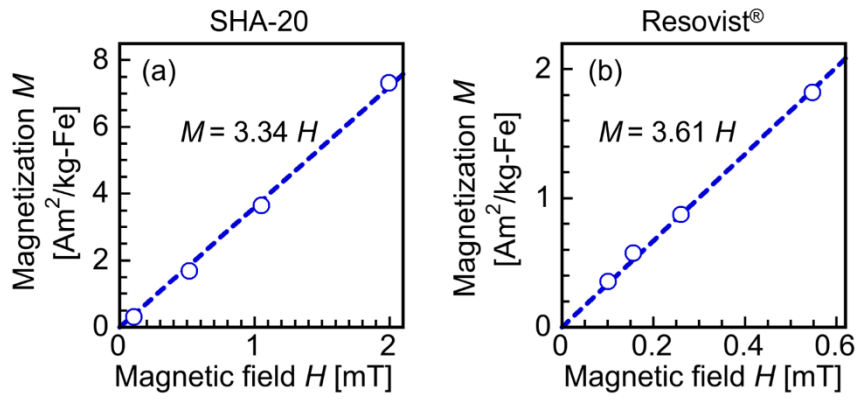


**Fig. S7** Magnetization measured under the DC magnetic field (plots) and the linear approximation of these plots (solid line) in (a) SHA-20 and (b) Resovist<sup>®</sup> in the solid.

#### Supplementary Note S4: Estimation of the magnetic relaxation time distribution

The magnetization response under a pulsed magnetic field is given by

$$PM_{cal}(t) = M_{max} \sum_{i=1}^{N_{A,\tau}} A_{M,\tau,i} \left\{ 1 - \exp\left(-\frac{t}{\tau_{R,i}}\right) \right\}, \#(S3)$$

where  $t$  is the time,  $\tau_R$  is the relaxation time,  $A_{M,\tau}$  is the magnetization fraction of  $\tau_R$ ,  $M_{max}$  is the maximum magnetization when the magnetization fully aligns with the applied magnetic field, and  $N_{A,\tau}$  is the number of points in  $A_{M,\tau}$  whose sum equals 1. In this estimation approach, the magnetization was normalized to the value at maximum  $t$  in the measurement. Training data for  $M_{pulse}$  to be fed into the NN were prepared by calculating  $A_{V,\tau}$  from the sum of three randomly selected Gaussian distributions with  $-11.0 < \log_{10} \tau < 0.0$  using Eq. (S1).

A deep learning framework was designed as shown in Fig. S8. The MSE was calculated as

$$MSE = \sum_{i=1}^{N_{train}} \left\{ \sum_{j=1}^{N_{out}} (A_{M,\tau,pred,i,j} - A_{M,\tau,train,i,j})^2 + \alpha_L \sum_{j=1}^{N_{in}} (PM_{cal,pred,i,j} - PM_{cal,train,i,j})^2 \right\}$$

where  $\alpha_L = 0.1$ . After the weights in the hidden layer of the NN were adjusted, the experimental  $A_{M,\tau}$  was analyzed by inputting the measured magnetic relaxation process. The predicted  $PM_{cal}$  was calculated from Eq. (S3) using the predicted  $A_{M,\tau}$ .

We employed the Adabelief optimizer,<sup>3</sup> and the NN model was trained using the open framework Pytorch with CUDA 11.8 on an NVIDIA Titan V GPU.

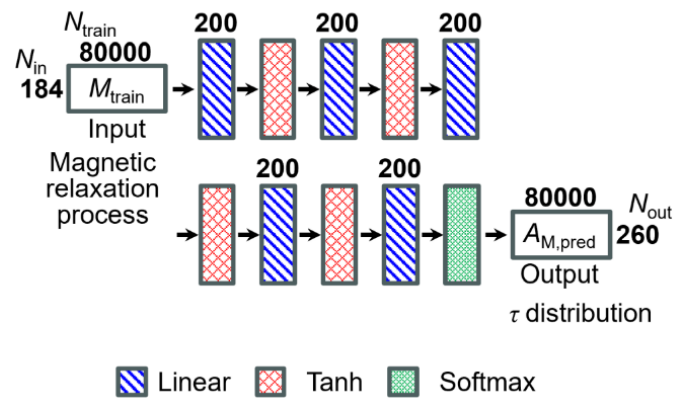


Fig. S8 Deep learning framework for estimating the distributions of the magnetic relaxation time  $\tau$  from the magnetic relaxation process.

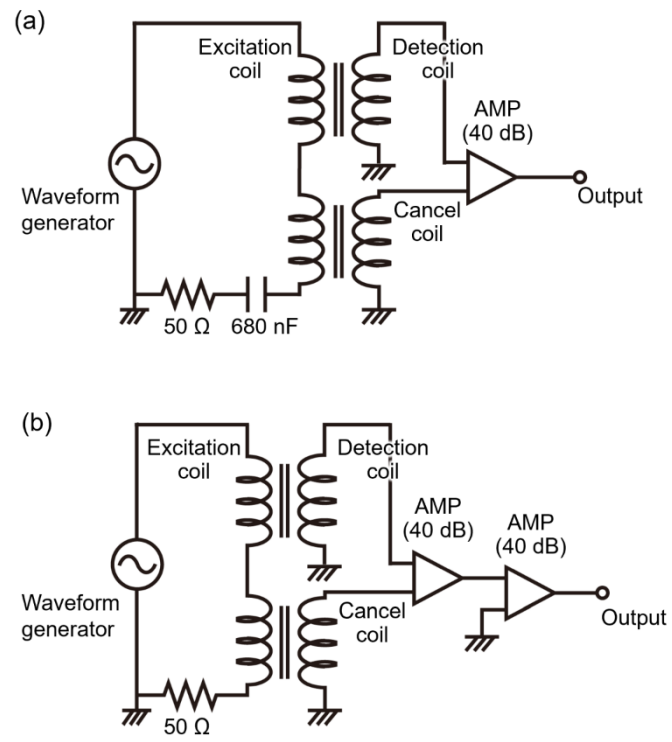


Fig. S9 Measurement circuit of (a) circuit (vi) and (b) circuit (vii) shown in Table S1.

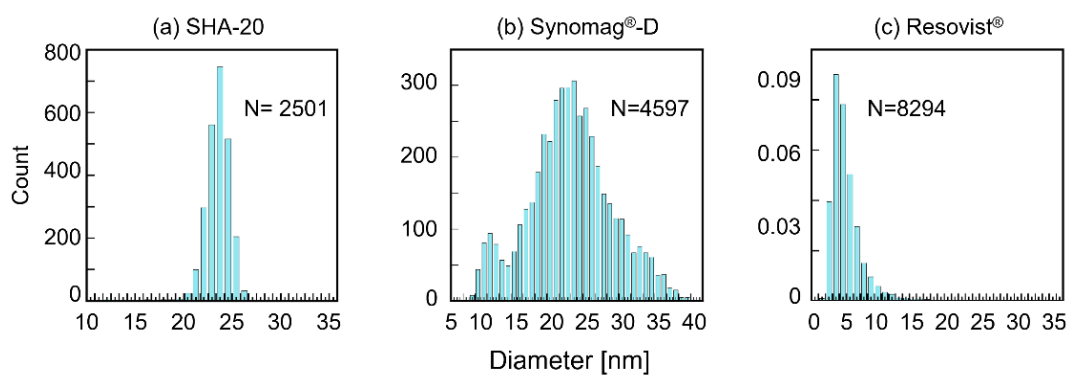


Fig. S10 Number of particles counted from TEM images for (a) SHA-20, (b) Synomag<sup>®</sup>-D, and (c) Resovist<sup>®</sup>

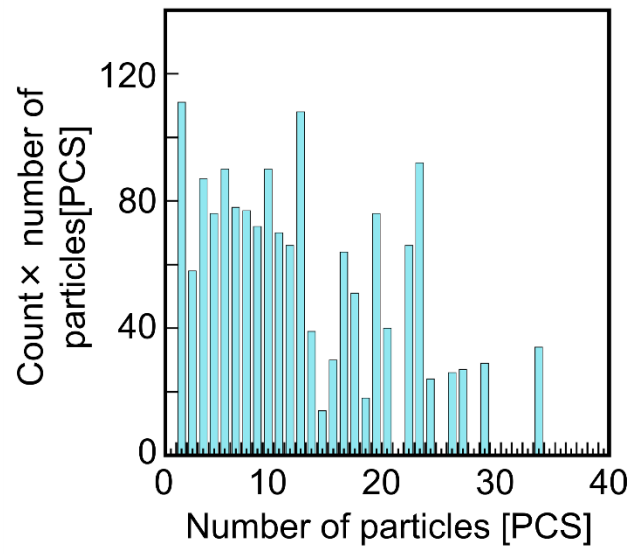


Fig. S11 Distribution density of the number of aggregated particles.

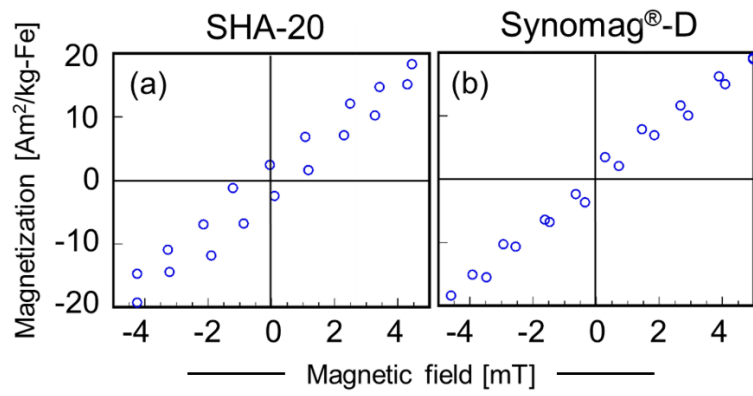


Fig. S12 DC magnetization curve with a magnified view in (a) SHA-20 and (b) Synomag<sup>®</sup>-D.

## References

- 1 T. Yoshida, N. B. Othman and K. Enpuku, *J. Appl. Phys.*, 2013, **114**, 173908.
- 2 S. Ota, H. Kosaka, K. Honda, K. Hoshino, H. Goto, M. Futagawa, Y. Takemura and K. Shimizu, *Adv. Mater.*, 2024, **36**, 2404766.
- 3 J. Zhuang, T. Tang, Y. Ding, S. C. Tatikonda, N. Dvornek, X. Papademetris and J. Duncan, *Adv. Neural Inf. Process. Syst.*, 2020, **33**, 18795.
- 4 T. Q. Bui, A. J. Biacchi, C. L. Dennis, W. L. Tew, A. R. H. Walker and S. I. Woods, *Appl. Phys. Lett.*, 2022, **120**, 012407.